Statistical Analysis and Classification of Acoustic Color Functions

J. Derek Tucker[a] and Anuj Srivastava[b]

[a]Naval Surface Warfare Center, Panama City Division, Panama City, FL, USA 32407
[b]Department of Statistics, Florida State University, Tallahassee, FL, USA 32306

ABSTRACT

In this paper we present a method for clustering and classification of acoustic color data based on statistical analysis of functions using square-root velocity functions (SVRF). The convenience of the SVRF is that it transforms the Fisher-Rao metric into the standard $\mathbb{L}^2$ metric. As a result, a formal distance can be calculated using geodesic paths. Moreover, this method allows optimal deformations between acoustic color data to be computed for any two targets allowing for robustness to measurement error. Using the SVRF formulation statistical models can then be constructed using principal component analysis to model the functional variation of acoustic color data. Empirical results demonstrate the utility of functional data analysis for improving performance results in pattern recognition using acoustic color data.

Keywords: acoustic color, functional data analysis, pattern recognition, shape analysis, sonar imagery

1. INTRODUCTION

The problem of underwater object detection and classification capture using sonar has attracted a substantial amount of attention.[1–5] This problem is complicated due to various factors such as variations in operating and environmental conditions, presence of spatially varying clutter, variations in target shapes, compositions and orientation. Moreover, bottom features such as coral reefs, sand formations, and vegetation may totally obscure a target or confuse the detection process. Consequently, a robust detection system should be able to quantify changes between the returns from the bottom and any target activity in sonar images, while at the same time extract useful features for subsequent classification. Thus, a robust system designed to mitigate false alarms in various clutter density scenarios will be desirable.

Considerable research has been devoted to the development of different detector and classification methodologies to detect and classify underwater objects utilizing sonar imagery. Dobeck[1,6] utilized a nonlinear matched filter to identify mine-size regions that match the target template in a side-scan sonar image. For each detected region, several features were extracted based on the size, shape, and strength of the target template. A stepwise feature selection process was then used to determine the subset of features that maximizes the probability of detection and classification. A k-nearest neighbor and an optimal discrimination filter classifier were used to classify each feature vector and the decisions of the two classifiers were fused to generate the final decision. In,[2] the adaptive clutter filter detector in[7] was individually applied to three different sonar images varying in frequency and bandwidth. Final classification is done using an optimal set of features using a nonlinear log-likelihood ratio test where the decisions of the individual detector and classifier are fused. Recently in[4] we developed a new coherence-based detection framework for dual-sensor problem using Canonical Coordinate Analysis (CCA) that can be applied to the data collected using two disparate sonar systems. Using this method allows for the simultaneous detection and feature extraction of coherent target information among two sonar images.

These methods all use traditional synthetic aperture sonar (SAS) images which often provides high quality images of proud targets which are useful for image based detection, localization, and identification algorithms; however, this is not the case for buried targets where images are usually blurred with less structure definition,

Approved for public release; distribution is unlimited
Further author information: (Send correspondence to Mr. J. Derek Tucker)
J. D. Tucker: E-mail: james.d.tucker@navy.mil, Telephone: 1 850 636 6090

and hence, target identification from these images is more difficult. Generating acoustic color data products is one way to overcome these shortcomings. Acoustic color[8,9] is a simple, spectral-based method that generates a normalized plot showing the strengths of the return signatures off an object in individual frequency bands at various aspects that may provide features useful for identification. The problem is then how does one do statistical analysis on these acoustic color images, which are essentially a two-dimensional function of frequency and aspect which represents target strength.

The solution to this problem is statistical functional data analysis. However, one must be aware of a problem that manifests itself when doing classification and pattern recognition problems on this type of data. The data can be sensitive to sensor placement and alignment between samples over a target. In some instances, it may be relatively easy to decide how to warp functions from different samples for proper alignment, however this can become quite cumbersome for large data-sets and tends to be done in a supervised fashion. In this paper, we present a framework for unified warping and comparison of function data using recent developments from shape theory in statistics and use it for the alignment and classification of acoustic color data. Using a differential geometric approach, our method unlike previous methods in functional data analysis, allows warping and analysis in a single step. In other words we are able to warp the functions, calculate metrics, and naturally decompose the x and y variability of the data in a efficient unsupervised manner. Moreover, under this framework a mapping called a square-root velocity function (SVRF) provides simplification of the metric where the standard Fisher-Rao metric becomes the standard $\mathbb{L}^2$ inner product and the standard cross-section statistical analysis becomes applicable. In this way, one calculate the mean of the SRVFs while optimizing over the warping of the mean function.

This paper is organized as follows: Section 2 presents and reviews the current theory in elastic function alignment and presents the Fisher Rao Metric and the method for warping the data. Section 3 presents the results of this method when applied to acoustic color data presenting both the warping and separability of the metric in feature space. Finally, conclusions and observations are offered in Section 4.

2. FUNCTION REPRESENTATION AND ALIGNMENT

This work is motivated by recent developments in statistical shape analysis of parameterized curves[10–12] in which we take a differential geometric approach to statistical functional analysis of elastic functions.[13] Consider any two functions $f_1, f_2 \in \mathcal{F}$, where $\mathcal{F}$ is an appropriate space of functions on [0,1], and $\gamma \in \Gamma$. The main problem solved in[13] is can we find a distance $d(\cdot,\cdot)$ on $\mathcal{F}$ such that $d(f_1, f_2) = d(f_1 \circ \gamma, f_2 \circ \gamma)$, for all f_1, f_2, and γ. The solution comes from a generalization of the square-root representation, which under this transformation the Fisher-Rao Riemannian metric becomes the $\mathbb{L}^2$ inner product and the standard cross-sectional functional analysis becomes applicable. Moreover, by computing the mean of the SRVFs we can provide an alignment of the individual functions to the mean and a covariance operator that can be further used for functional principal component analysis (FPCA). The important aspect of this method is that all the analysis of computing statistics, modeling, principal components is performed in the $\mathbb{L}^2$ space of SRVFs and the final results are converted back to the original function space. The reasons for this is that the $\mathbb{L}^2$ metric is a proper distance for analyzing SRVFs of elastic functions and allows for a formal statistical analysis. The method will be briefly described below, for a more in-depth discussion see.[13]

2.1 Pairwise Alignment Problem

Let Γ be the group of all warping functions

$$\Gamma = \{\gamma : [0,1] \to [0,1] | \gamma(0) = 0, \gamma(1) = 1, \gamma \text{ is a diffeomorphism}\} \tag{1}$$

and it acts on the function space by composition $(f, y) = f \circ \gamma$. It is common to use the the following function for alignment

$$\min_{\gamma \in \Gamma} ||f_1 \circ \gamma - f_2|| \tag{2}$$

which however is not a distance function and is not symmetric which inhibits the definition of any statistical measures. It can however be made symmetric by using double optimization, but still fails in being a distance function to due lack of isometry. The solution to this problem is the Fisher-Rao distance.

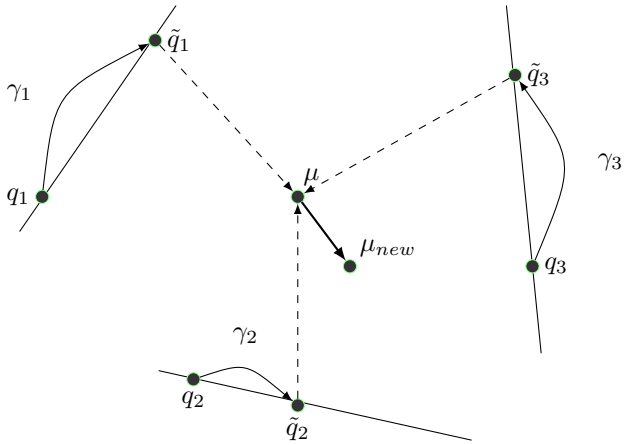

Figure 1. Ensemble alignment problem.

2.2 Fisher Rao Metric

Let f represent a real-valued continuous function on the interval [0,1] and let $\mathcal{F}$ denote the set of all such functions. For any $v_1, v_2 \in T_f(\mathcal{F})$, the Fisher-Rao Riemannian Metric is defined as

$$\langle\langle v_1, v_2 \rangle\rangle_f = \frac{1}{4} \int_0^1 \dot{v}_1(t) \dot{v}_2(t) \frac{1}{|\dot{f}(t)|} \, dt \tag{3}$$

which is invariant to re-parameterization, $\langle\langle v_1, v_2 \rangle\rangle_f = \langle\langle (v_1 \circ \gamma), (v_2 \circ \gamma) \rangle\rangle_{f \circ \gamma}$ and leads to the Fisher-Rao distance

$$d_{FR}(f_1, f_2) = \inf_{\alpha:[0,1]\to\mathcal{F}, \alpha(0)=f_1, \alpha(1)=f_2} \left(\int_0^1 (\langle\langle \dot{\alpha}(\tau), \dot{\alpha}(\tau) \rangle\rangle_{\alpha(\tau)})^{1/2} \, d\tau \right). \tag{4}$$

This distance satisfies, $d_{FR}(f_1, f_2) = d_{FR}(f_1 \circ \gamma, f_2 \circ \gamma)$ and is invariant to domain warping, however it is difficult to compute and only a few numerical solutions attempt to solve it.

We can overcome this problem by defining a mapping

$$Q(x) \equiv \begin{cases} x/\sqrt{|x|} & \text{if } |x| \neq 0 \\ 0 & \text{otherwise.} \end{cases} \tag{5}$$

For studying f, we will represent it using the SRVF defined as $q : [0, 1] \to \mathbb{R}$, where $q(t) \equiv Q(\dot{f}(t)) = \dot{f}(t)/\sqrt{|\dot{f}(t)|}$ and if f is continuous, then q is square-integrable. The SVRF can then be reparameterized by $(q, \gamma) = (q \circ \gamma)\sqrt{\dot{\gamma}}$ and the space of all SVRFs is $\mathbb{L}^2([0, 1], \mathbb{R})$ or $\mathbb{L}^2$. Therefore, under the SVRF representation of f, the Fisher-Rao Riemannian metric becomes the $\mathbb{L}^2$ distance, i.e., $d_{FR} = ||q_1 - q_2||$. The proof of which can be found in.[13] Moreover, for any two SVRFs $q_1, q_2 \in \mathbb{L}^2$ and $\gamma \in \Gamma$, we have $||(q_1, \gamma) - (q_2, \gamma)|| = ||q_1 - q_2||$.

2.3 Ensemble Alignment

Now that the Fisher-Rao distance on $\mathcal{F}$ has been defined, we can now define the warping framework to align the functions horizontally to improve the matching of features (peaks and valleys) across functions. In the SVRF framework this is accomplished naturally using Karcher mean. If we define $\mathcal{S}$ to be the quotient space $\mathcal{S} = \mathbb{L}^2/\Gamma$, then $\mathcal{S}$ is the set of all orbits of an SVRF; $[q] = \text{closure}\{(q, \gamma)|\gamma \in \Gamma\}$. We can then align the functions by computing a mean function in $\mathcal{S}$ and during that process we warp the SRVFs of the given functions to match the mean function. A graphical diagram of this process is given in Figure 1.

Lets define a distance function on $\mathcal{S}$

$$d_0([q_1], [q_2]) = \min_{\gamma \in \Gamma} ||q_1 - (q_2 \circ \gamma)\sqrt{\dot{\gamma}}|| \tag{6}$$

which is a proper distance function and the Karcher mean can be computed using this distance function in

$$\mu = \arg\min_{q \in \mathbb{L}^2} d_0([q], [q_i])^2. \tag{7}$$

The above optimization problem can be solved by the following algorithm which relies on dynamic programming.

Algorithm 1: Karcher Mean of SRVFs

1. Initialization: Select $\mu = q_i$ for some $i \in \{1, 2, \ldots, n\}$
2. For each $q_i,\ i = [1, 2, \ldots, n]$ compute the optimal warping function

$$\gamma_i^* = \arg\min_{\gamma \in \Gamma} ||\mu - (q_i \circ \gamma)\sqrt{\dot{\gamma}}|| \tag{8}$$

   which can be solved using dynamic programming.

3. Compute the aligned SRVFs $\tilde{q}_i = (q_i \circ \gamma_i^*)\sqrt{\dot{\gamma}_i^*}$
4. If the increment, $||\frac{1}{n}\sum_{i=1}^n \tilde{q}_i - \mu||$ is small, then continue. Else update the mean $\mu \mapsto \frac{1}{n}\sum_{i=1}^n \tilde{q}_i$ and return to step 2.

This algorithm results in the Karcher mean μ, the aligned SRVFs $\{\tilde{q}_i\}$, and the optimal warping functions $\{\gamma_i^*\}$. We can then convert the aligned SRVFs to aligned functions using

$$\tilde{q}_i \mapsto \tilde{f}_i(t) \equiv f_i(0) + \int_0^t \tilde{q}_i(s)|\tilde{q}_i(s)|\, ds \tag{9}$$

and we now have the desired components: the y variability $\{\tilde{f}_i\}$ and the x variability $\{\gamma_i^*\}$. In the SRVFs we can then calculate proper distances, metrics, perform classification, and perform function principal component analysis and impose probability models on the coefficients and then bring the results back to the function space using integration.

3. EXPERIMENTAL RESULTS

In this section, we describe some experimental results to demonstrate the use of this elastic functional analysis on acoustic color data. First, we present results of the warping of the acoustic color data and how it improves feature alignment. Second, results showing the separability of the warped data over the original data and classification rates between the two using the $\mathbb{L}^2$ metric defined in Section 2 and calculated using SRVFs.

3.1 Data Description

The data used in these experiments was collected at the NSWC PCD test pond. For a description of the pond and experimental setup the reader is referred to.[14] The raw sonar data was collected using a 1 - $30kHz$ LFM chirp and data was collected for a 11 proud targets that included a solid aluminum cylinder, an aluminum pipe, an inert $81mm$ mortar (filled with cement), a solid steel artillery shell, two machined aluminum UXOs, a machined steel UXO, a de-militarized $152mm$ TP-T round, a de-militarized $155mm$ empty projectile (without fuse or lifting eye), a small aluminum cylinder with a notch, and two rocks with sizes comparable to the UXO targets. The aluminum cylinder is $2ft$ long with a $1ft$ diameter; while the pipe is $2ft$ long with an inner diameter of $1ft$ and 3/8 inch wall thickness.

The acoustic color data was generated from the raw sonar data to construct target strength as a function of frequency and aspect angle. Due to the relatively small separation distances between the targets in the experimental setup, the scattered fields from the targets overlap. To generate the acoustic templates, SAS images were formed and then an inverse imaging technique was used to isolate the response of an individual

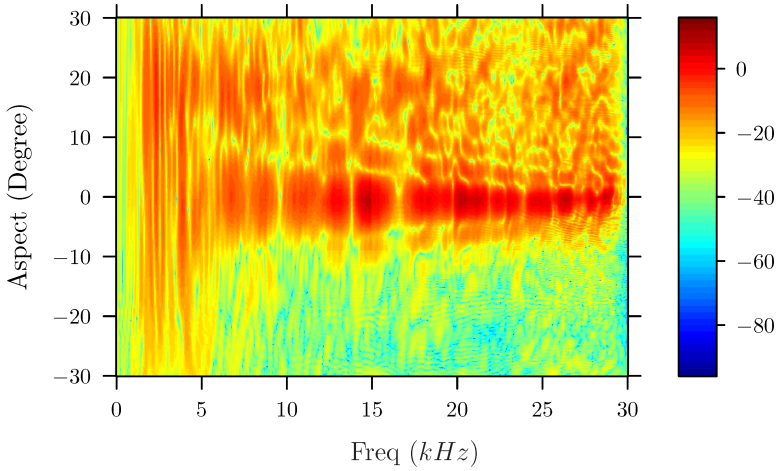

(a) Aluminum Pipe Pass #1

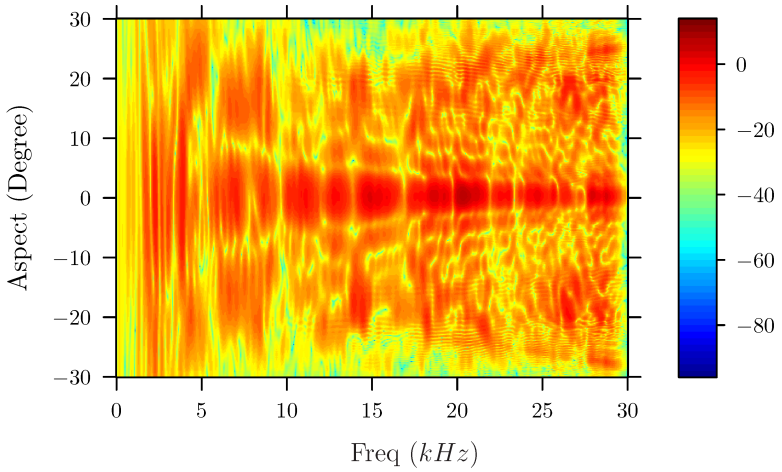

(b) Aluminum Pipe Pass #2

Figure 2. Example acoustic color map for the aluminum pipe for two different target passes.

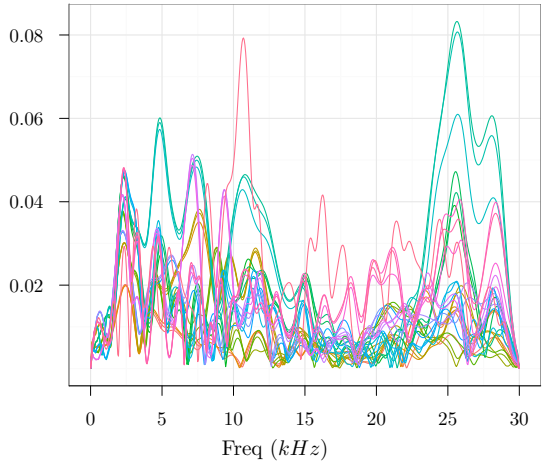

(a) Original Data (f)

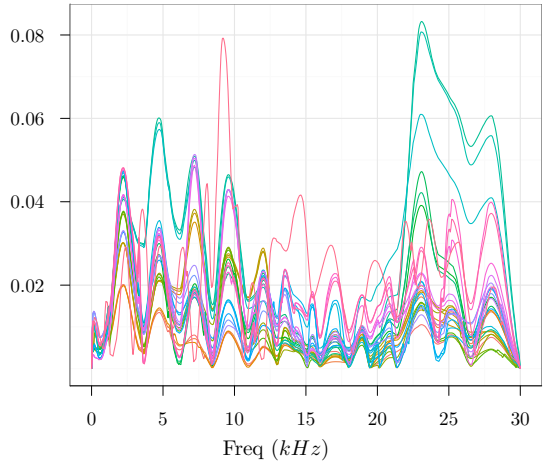

(b) Warped Data ($\tilde{f}$)

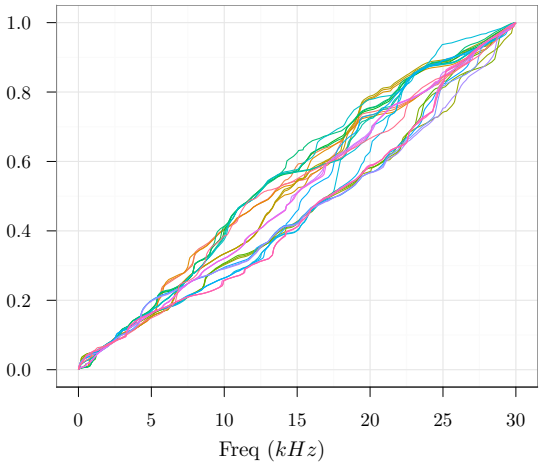

(c) Warping Function (γ_i^*)

Figure 3. Original data and aligned functions for aluminum pipe at 0° aspect.

target and to suppress reverberation noise. A brief summary of this process is as follows: The raw sonar data is matched filtered and the SAS image is formed using the $\omega - k$ beamformer.[15] The target is then located in the SAS image and is then windowed about selected location. This windowed image contains the information to reconstruct the time signals associated with a given target via inverting the $\omega - k$ beamformer.[16]

From the 11 targets, 9 different data collections runs were done, and 99 acoustic color templates were generated using the method described above, see Figure 2 for an example acoustic color map for the aluminum pipe for two different data collection runs. From the acoustic color maps, one-dimensional functional data was generated by taking slices at aspect values of $-10°, 0°, 10°$ and therefore generating 297 data samples. The two figures look similar, however there are discrepancies between the two maps notably at larger aspect angles and the magnitude of the function. These discrepancies and misalignment can greatly inhibit classification performance.

3.2 Data Warping

The first results we present are the warping results on an example object from the above described data set. Figure 3a presents the original target strength acoustic curves for the aluminum pipe at 0° aspect. These

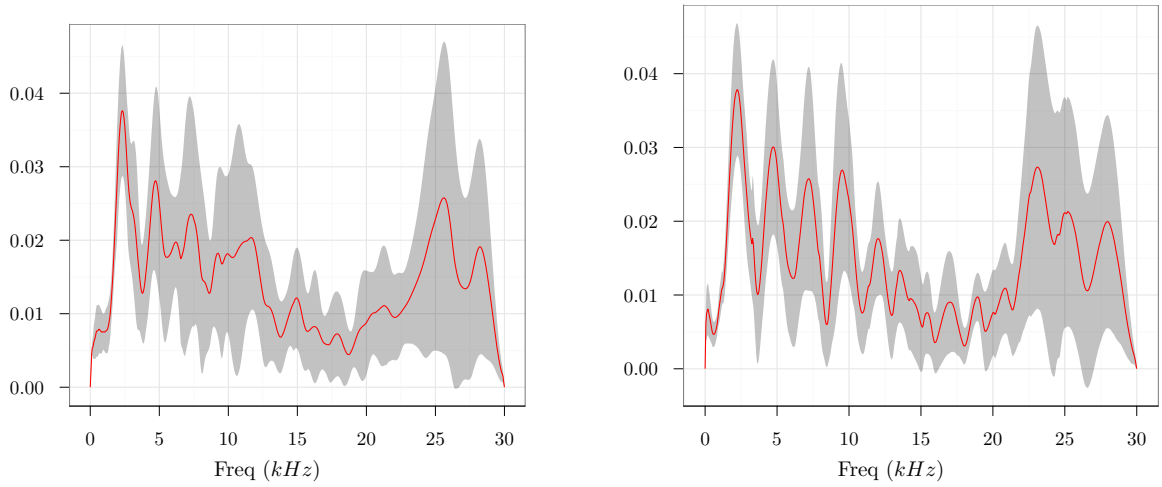

(a) Original Data Mean ± STD (b) Warped Data Mean ± STD

Figure 4. Original data and aligned functions statistics at 0° aspect.

represent 27 different target passes over the aluminum pipe and are one slice from the acoustic color map. The frequency dependent target strength functions are somewhat similar, but we can see variations in strength and small shifts in location of the features of the function (i.e., peaks and valleys).

Figure 3b presents the resulting aligned function $\{\tilde{f}_i\}$ using Algorithm 1 presented in Section 2.3 and Figure 3c presents the corresponding warping functions $\{\gamma_i^*\}$. The plots of $\{\tilde{f}_i\}$ show tighter alignment of the functions with more defined peaks and valleys, representing more tighter alignment of the measured data of the same physical phenomena. Figure 4a and 4b present the cross-sectional mean ± standard deviation of the original and warped data, respectively. The difference between the original and warped data can be noted by the spread of the standard deviation from the mean and for the warped data it is much tighter with the peaks more defined around certain frequencies.

3.3 Object Clustering and Classification

Next, we present the results of object clustering and classification of the 11 objects in the acoustic color data set. The first step in processing was each object was aligned in class using Algorithm 1. After the aligned data and warping functions were calculated the distance between each of the functions in the data set was calculated using d_0 and was done in SVRF space where the distance is easily calculated using the $\mathbb{L}^2$ metric. Figure 5a and 5b presents the symmetric distance matrix containing the pairwise distances for the original data $\{q_i\}$ and the warped data $\{\tilde{q}_i\}$, respectively. It can easily be seen from the matrices there is a definite separation in Figure 5b over Figure 5a where the distances in class have been decreased and distances out of class have been increased. There still remains a few difficult separation points for the aluminum pipe and solid aluminum cylinder.

The distance matrices in Figure 5 are clustered using their 3-D embeddings for two different manifold learning techniques, multidimensional scaling (MDS) and Diffusion Maps to demonstrate the discriminating ability of these two metrics. Figure 6 shows the results for the original and warped data using both MDS and diffusion maps. For the original data, we can see that MDS was able to separate only one of the 11 objects and there is no separation for diffusion map. However after alignment using developed algorithm, both methods have excellent clustering results for both embedding techniques.

Figure 7a and 7b presents the precision versus recall plots for the original and warped data, respectively. Precision is defined to be the true positive rate divided by the sum of the true positive rate and false positive rate and where recall is defined to be true positive rate divided by the sum of the true positive rate and the false negative rate. In a classification task, a precision score of 1.0 for a class C means that every item labeled as belonging to class C does indeed belong to class C (but says nothing about the number of items from class

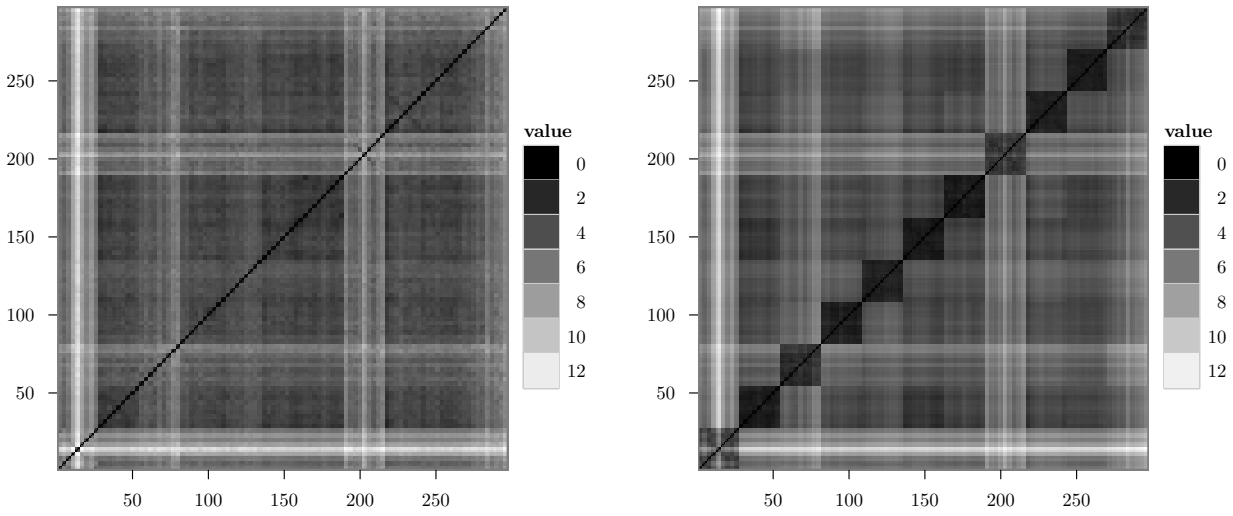

(a) Original Data (q) (b) Warped Data ($\tilde{q}$)

Figure 5. Pairwise distance matrices calculated using d_0.

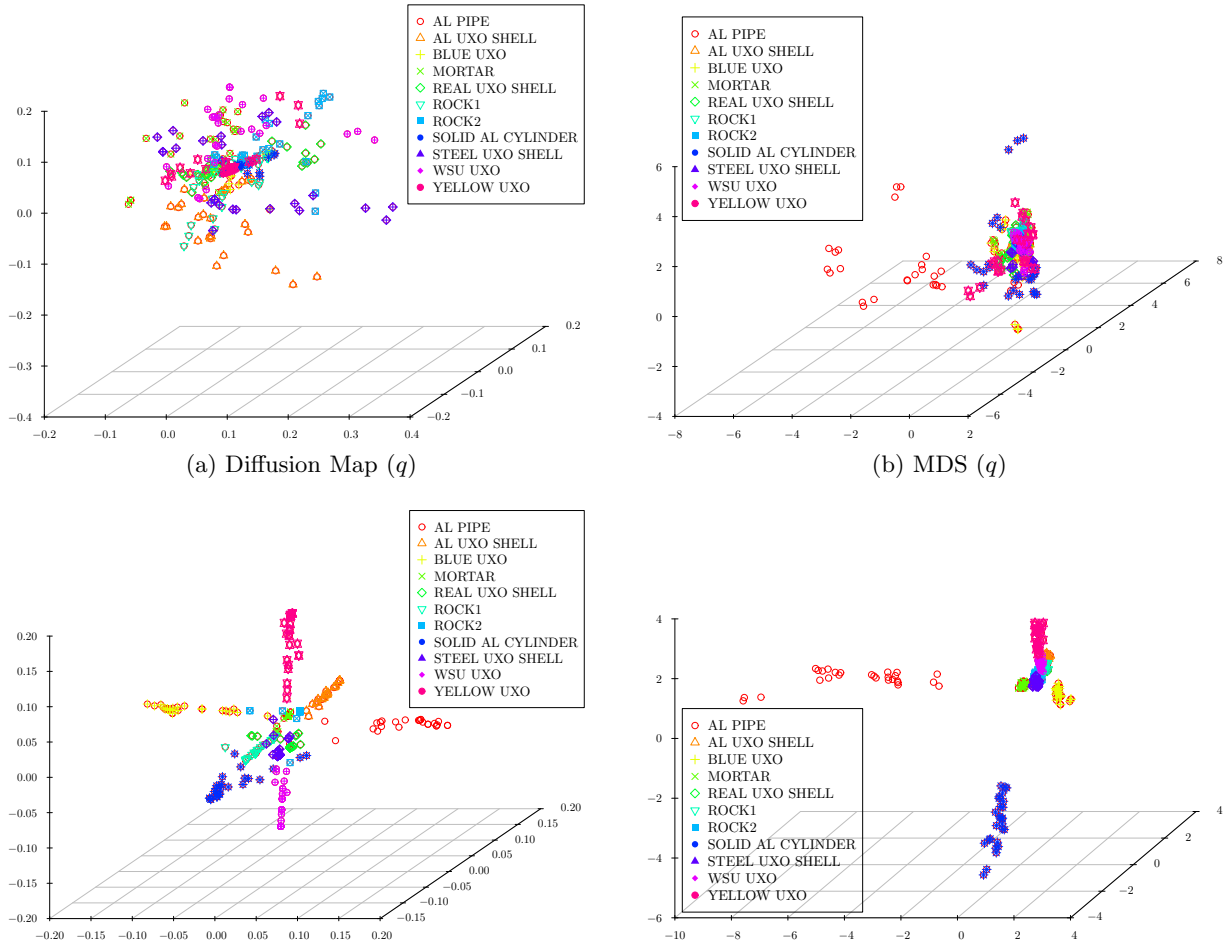

(a) Diffusion Map (q) (b) MDS (q)

(c) Diffusion Map ($\tilde{q}$) (d) MDS ($\tilde{q}$)

Figure 6. Target clusters for acoustic color metric using d_0.

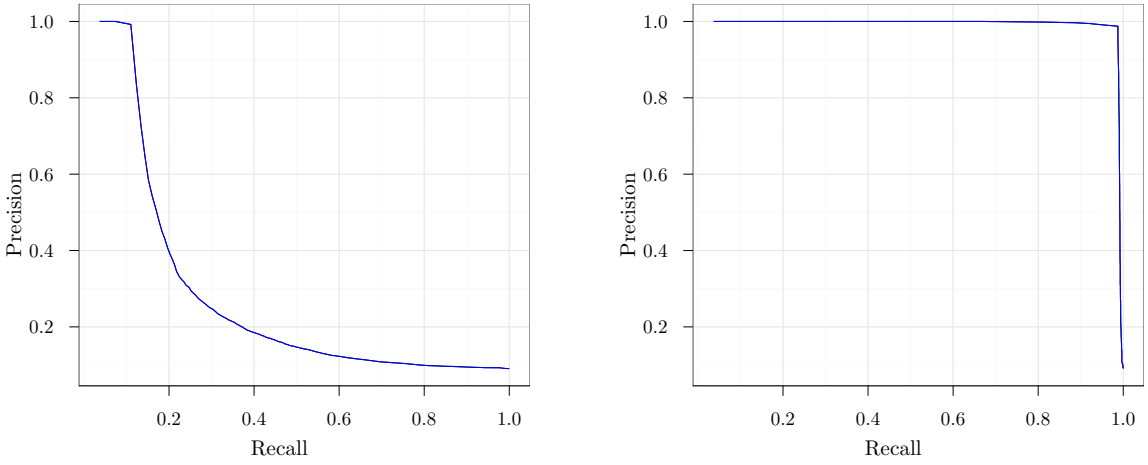

(a) Original Data (f) (b) Warped Data ($\tilde{f}$)

Figure 7. Precision versus recall plot for pairwise distance calculated using d_0.

C that were not labeled correctly) whereas a recall of 1.0 means that every item from class C was labeled as belonging to class C (but says nothing about how many other items were incorrectly also labeled as belonging to class C).

By examining Figure 7a the precision recall plot drops off very rapidly for a low recall demonstrating a very lackluster classification performance of the original data using the distance metric. However, after warping and alignment and using the geodesic distance the performance is increased to nearly 99% which is demonstrated in Figure 7b which shows a nearly perfect precision recall plot.

4. CONCLUSIONS AND OBSERVATIONS

The statistical analysis and classification of acoustic color data is a challenging task. We have proposed a novel approach for the classification of acoustic color using elastic functional data analysis with a new approach from the emerging field of shape analysis curves. We have demonstrated a method which aligns the data and a way to easily calculate a proper Riemannian distance between functions, which may be used for classification purposes. Aligning the data allows one to overcome measurement error between target passes and preliminary results on the provided data set show good separation among targets in feature space.

ACKNOWLEDGMENTS

This work was supported by the NSWC PCD In-house Laboratory Independent Research program funded by the Office of Naval Research.

REFERENCES

1. G. J. Dobeck, "Image normalization using the serpentine forward-backward filter: application to high-resolution sonar imagery and its impact on mine detection and classification," *Proc. SPIE* **5734**, pp. 90–110, April 2005.
2. T. Aridgides and M. Fernandez, "Image-based ATR utilizing adaptive clutter filter detection, LLRT classification, and volterra fusion with application to side-looking sonar," *Proc. SPIE* **7664**, pp. 1R–11R, March 2010.
3. N. Klausner, M. R. Azimi-Sadjadi, and J. D. Tucker, "Multi-sonar target detection using multi-channel coherence analysis," *Proc. of MTS/IEEE Oceans 2010 Conference* , pp. 1–7, Sept. 2010.

4. J. D. Tucker, N. Klausner, and M. R. Azimi-Sadjadi, "Target detection in m-disparate sonar platforms using multichannel hypothesis testing," *Proc. of MTS/IEEE Oceans 2008 Conference* , pp. 1–7, Sep. 2008.
5. J. D. Tucker, J. T. Cobb, and M. R. Azimi-Sadjadi, "Generalized likelihood ratio test for finite mixture model of K-distributed random variables," *IEEE Digital Signal Processing Workshop* **to be published**, Jan 2011.
6. G. J. Dobeck, "Fusing sonar images for mine detection and classification," *Proc. SPIE* **3710**, pp. 602–614, April 1999.
7. T. Aridgides, P. Libera, M. Fernandez, and G. J. Dobeck, "Adaptive filter/feature orthogonalization processing string for optimal LLRT mine classification in side-scan sonar imagery," *Proc. SPIE* **2765**, pp. 110–121, April 1996.
8. N. Intrator, N. Neretti, and Q. Huynh, "Sonar object discriminiation via spectral density analysis," *Proc. of MTS/IEEE OCEANS 2004 Conference* **2**, pp. 740–742, Nov 2004.
9. D. Miklovic and M. Bird, "Quantitative acoustic color displays for classification with broadband sonars," *Proc. of MTS/IEEE Oceans 1998 Conference* **1**, pp. 592–597, Sept. 1998.
10. L. Younes, "Computable elastic distance between shapes," *SIAM Journal of Applie Mathematics* **58**(2), pp. 565–586, 1998.
11. L. Younes, P. W. Michor, J. Shah, D. Mumford, and R. Lincei, "A metric on shape space with explicit geodesics," *Matematica E Applicazioni* **19**(1), pp. 25–27, 2008.
12. A. Srivastava, E. Klassen, S. H. Joshi, and I. H. Jermyn, "Shape analysis of elastic curves in euclidean spaces," *IEEE Trans. on Pattern Analysis and Machine Intelligence* **accepted for publication**, 2010.
13. A. Srivastava, W. Wu, S. Kurtek, E. Klassen, and J. S. Marron, "Statistical analysis and modeling of elastic functions," *Journal of American Statistical Association* **submitted**, 2010.
14. S. Kargl, K. Williams, T. Marston, J. Kennedy, and J. Lopes, "Acoustic response of unexploded ordnance (uxo) and cylindrical targets) and cylindrical targets," *Proc. of MTS/IEEE Oceans 2010 Conference* , pp. 1 –5, 2010.
15. M. Soumekh, *Synthetic Aperture Radar Signal Processing*, Wiley, 1999.
16. A. Khwaja, L. Ferro-Famil, and E. Pottier, "Sar raw data simulation using high precision focusing methods," *European Radar Conference* , pp. 33 –36, 2005.